published by Ural Federal University
eISSN 2411-1414
chimicatechnoacta.ru

ARTICLE
2025, vol. 12(2), No. 12209
DOI: 10.15826/chimtech.2025.12.2.09

Transport and structural properties of $(CH_3)_4NBF_4$ with nanodiamonds filler

Ivan Stebnitskii [ab] *, Yulia Mateyshina [ab], Nikolai Uvarov [ab]

a: Institute of Solid State Chemistry and Mechanochemistry, Siberian Branch of the Russian Academy of Sciences, Novosibirsk 630090, Russia
b: Department of Natural Sciences, Novosibirsk State University, Novosibirsk 630090, Russia
* Corresponding author: i.stebnitskii@g.nsu.ru

Abstract

Composite solid electrolytes are promising materials for electrochemical devices. The most interesting ionic components for them are salts of substituted ammonium due to their high thermal and electrochemical stability, but the properties of composites based on them are poorly understood. Composite solid electrolytes based on the substituted ammonium salt $(CH_3)_4NBF_4$ with highly dispersed nanodiamonds C_{ND} with specific surface area S_{sp} = 300±20 m²/g in a wide range of filler concentrations have been synthesized for the first time. It was found by X-ray diffraction method that the introduction of C_{ND} leads to the amorphization of the salt. The highest conductivity values are characterized by the composite $0.03(CH_3)_4NBF_4 - 0.97C_{ND}$ (σ = $4.2 \cdot 10^{-3}$ S/cm at 300 °C), whose electrical conductivity is 3-4 orders of magnitude higher than that of the original salt. Modeling the concentration dependence of the electrical conductivity of the composites using the mixing equation showed that the reason for the increase in electrical conductivity is the formation of an amorphous salt layer, the electrical conductivity of which is 4–5 orders of magnitude higher than that of the crystalline phase $(CH_3)_4NBF_4$.

Key findings

- The use of nanodiamonds C_{ND} with S_{sp} = 300±20 m²/g as a filler leads to the amorphization of $(CH_3)_4NBF_4$.
- $0.03(CH_3)_4NBF_4 - 0.97C_{ND}$ (σ = $4.2 \cdot 10^{-3}$ S/cm at 300 °C) has the highest conductivity, increasing the conductivity of a relatively pure salt by 3–4 orders of magnitude.
- The reason for the increased conductivity in composites is the formation of a highly conductive amorphous salt layer.

Accompanying information

Article history
Received: 20.01.25
Revised: 06.02.25
Accepted: 06.02.25
Available online: 12.02.25

Keywords
Substituted ammonium salts; tetramethylammonium tetrafluoroborate; nanodiamonds; transport properties

Funding
None.

Supplementary information
Transparent peer review: READ

Sustainable Development Goals
7 AFFORDABLE AND CLEAN ENERGY

1. Introduction

Composite solid electrolytes are promising materials for use in electrochemical energy storage [1–3]. They possess the best properties of ceramic electrolytes (high ionic conductivity, thermal stability) and polymer electrolytes (ability to withstand large deformations without destruction, ensuring stable contact with electrodes), while minimizing their risks (such as flammability and chemical instability) [4–6].

Composite electrolytes are heterogeneous systems consisting of an ionic compound and a heterogeneous additive. Inert fillers, which are dielectric nanoscale particles such as MgO, Al_2O_3, or non-conductive porous particles such as SiO_2 or metal-organic frameworks, are often used as additives [7–9]. The addition of such particles to ionic crystals leads to the formation of additional point defects near the interface, resulting in an increase in ionic conductivity by 1–4 orders of magnitude relative to the original compound [10–12].

The fundamental physicochemical properties of composite electrolytes are also influenced by the properties of the ionic compound itself. Substituted ammonium salts are considered a promising basis for composites because they often have high thermal and electrochemical stability, plasticity that can provide good contact with electrodes, and relatively high ionic conductivity in high-temperature phases [13–15]. These compounds can be used to create all solid-

state electrochemical devices [16, 17]. For example, recently, N,N-dimethylpyrrolidinium fluorohydrogenate was used as a solid electrolyte for a supercapacitor with graphite electrodes: the capacitance of the positive and negative electrodes was 263 F g^{-1} and 221 F g^{-1}, respectively, on the 300th cycle at a current density of 238 mA g^{-1} [18]. However, in most cases, the direct use of substituted ammonium salts in devices is complicated by low ionic conductivity (often less than 10^{-5} S/cm).

The introduction of nanosized particles can increase the electrical conductivity of substituted ammonium salts [19, 20]. Previously, we demonstrated that the conductivity of tetrafluoroborate tetrabutylammonium $(C_4H_9)_4NBF_4$ can be increased by 1.5-3 orders of magnitude in this way, with the relative increase in conductivity depending on the nature of the heterogeneous additive [21]. The largest effect was achieved with nanodiamonds C_{ND} (σ_{max} = 1.2·10^{-3} S/cm at 150 °C) [22]. Such composites with improved transport properties can be used as materials in supercapacitors. Thus, the fundamental possibility of creating a supercapacitor with an electrolyte of $0.6(C_2H_5)_3CH_3NBF_4$ – $0.4C_{ND}$, demonstrating a capacity of 40 F g^{-1} at a voltage scanning rate of 5 mV s^{-1}, was previously shown.

However, to date, there has been little investigation of how the salt properties affect the physicochemical properties of such composites. Therefore, in this work, the system $(CH_3)_4NBF_4$–C_{ND} was investigated for comparison with previously studied composites based on substituted ammonium salts with nanodiamonds addition.

2. Materials and methods

2.1. Materials

Tetramethylammonium tetrafluoroborate $(CH_3)_4NBF_4$ was synthesized by an exchange reaction in aqueous solution between tetramethylammonium chloride $(CH_3)_4NCl$ (Sigma Aldrich, reagent grade) and tetrafluoroboric acid HBF_4 (Sigma Aldrich, 48 wt.%), taken in stoichiometric amounts. The resulting white precipitate $(CH_3)_4NBF_4$ was washed with water to pH 7 to remove any residual HBF_4 and then dried at 100 °C under reduced pressure.

Commercial UDA-C nanodiamonds (S_{sp} = 300±20 m^2/g, produced by the Altai Federal Research and Production Center, Biysk, Russia) were used in this work. Before use, nanodiamonds C_{ND} were preheated at 300 °C for 3 h to remove unstable functional groups and adsorbed water molecules. The specific surface area of the preheated nanodiamonds was determined by nitrogen adsorption method using ThermoSorb TPD 1200, degassing mode: 60 min at 250 °C, according to the 5-point method in the pressure range p/p_o= 0.2–0.4.

Composites $(1–x)(CH_3)_4NBF_4$ – xC_{ND} ($0 < x < 1$, x – mole fraction) were prepared by mixing stoichiometric amounts of salt and nanodiamonds with the addition of acetonitrile as a solvent, followed by heating the samples in a drying oven at 200 °C for 1 h to remove the residual solvent.

2.2. Methods

The thermal properties of the composites were investigated using a differential scanning calorimeter DSC-500 (SamSTU, Russia). For this purpose, samples of known mass (5–15 mg) were placed in aluminum crucibles, tightly packed and heated in the temperature range of 20–300 °C at a heating rate of 10 °C/min in an argon stream.

The structural properties of $(CH_3)_4NBF_4$ and composites based on it were investigated by X-ray diffraction on a D8 Advance diffractometer (Bruker, Germany) using Cu Kα radiation with a Kβ filter. The diffractograms were recorded in the angular range 10°<2θ<90° with a step Δ2θ = 0.0195°, and a one-dimensional Lynx-Eye detector was used to detect the diffraction rays. The diffractograms were analyzed using the GSAS-II program [23].

The surface morphology of the composite tablet samples was analyzed using a Hitachi TM 1000 scanning electron microscope (Oxford Instruments Analytical Ltd.).

To investigate the transport properties, the composite powders were compacted with two Ag-electrodes at a pressure of 100 MPa. The compacted powders were tablets with a diameter of about 6.3 mm and a thickness of 0.7–2 mm. The density of pure $(CH_3)_4NBF_4$ salt compressed into a tablet exceeds 96% of the theoretical density; taking into account the plasticity of the salt, the density of the composites exceeds 90%. The electrical properties were measured by impedance spectroscopy in low vacuum with a residual pressure of 50 mTorr in the mode of staggered isotherms in the temperature range of 100–300 °C using a two-electrode circuit on a Hewlett Packard HP 4284A Precision LCR Meter (Hewlett-Packard, Japan) in the range of 30 Hz – 1 MHz. The obtained impedance hodographs were analyzed using Zview software (version 3.1, Scribner Associates, Inc., USA) to determine the total resistance R. The total ionic conductance was calculated using the formula $\sigma = d/(R \cdot S)$, where d and S are the diameter and area of the tablet, respectively.

3. Results and Discussion

3.1. Thermal properties

According to the study of G. Zabinska et. al. $(CH_3)_4NBF_4$ undergoes phase transitions at –119 °C and at 328 °C [24]. Matsumoto et. al. confirmed the presence of a high temperature phase transition (at 333 °C) and also noted that an exothermic effect at temperatures above 378 °C caused by the decomposition of the salt [25].

In the temperature range investigated (20–300 °C), neither endothermic nor exothermic peaks were found for the pure $(CH_3)_4NBF_4$ salt and for the $(CH_3)_4NBF_4$ – C_{ND} composites, indicating that the salt is in the same phase in all samples and that the salt and composites will be stable during the high temperature studies (Figure 1).

3.2. Structural and microstructural properties

The pure salt $(CH_3)_4NBF_4$ was indexed at room temperature within the P4/nmm space group ($a = b$ = 8.284(5) Å,

 DOI: 10.15826/chimtech.2025.12.2.09

c = 5.914(9) Å, R_{wp} = 10.2 %), which is consistent with previous single crystal X-ray diffraction studies (P4/nmm, $a = b$ = 8.231(3) Å, c = 5.889(3) Å [26]) as well as powder X-ray diffraction (PDF 482173: P4/nmm, $a = b$ = 8.257 Å, c = 5.912 Å [26]).

The X-ray diffraction patterns of the composites $(1–x)(CH_3)_4NBF_4 – xC_{ND}$ (Figure 2) show reflections of the salt phase, stable at room temperature, and a broad maximum near 2θ ≈ 43.7°, which belongs to the (111) reflection of the diamond phase Fd-3m.

It is known that X-ray diffraction is sensitive to the volume of the phase trapped under the beam, so for correct analysis of the change in intensity of the peaks with the composition, the mole fractions of nanodiamonds were converted to volume fractions by the formula:

$$f = \frac{x}{x + (1-x)\frac{M_1\rho_2}{M_2\rho_1}}, \quad (1)$$

where x and f are the molar and volume fractions of C_{ND} nanodiamonds, respectively, M_1 and M_2 are the molar masses of salt and C_{ND}, respectively, and ρ_1 = 1.34 g/cm³ and ρ_2 = 3.5 g/cm³ are the densities of salt and C_{ND}, respectively.

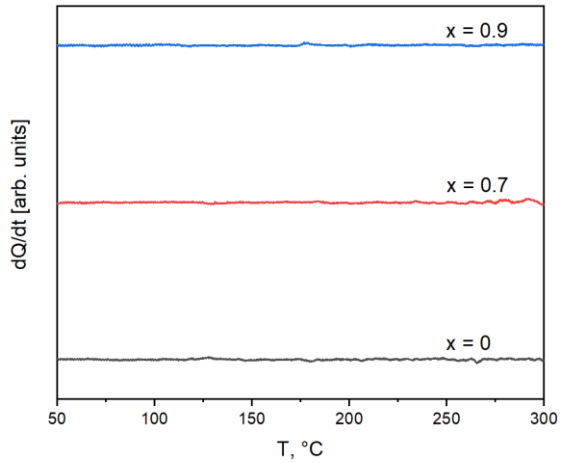

Figure 1 DSC curves for $(1–x)(CH_3)_4NBF_4 – xC_{ND}$ (x = 0, 0.7, 0.9).

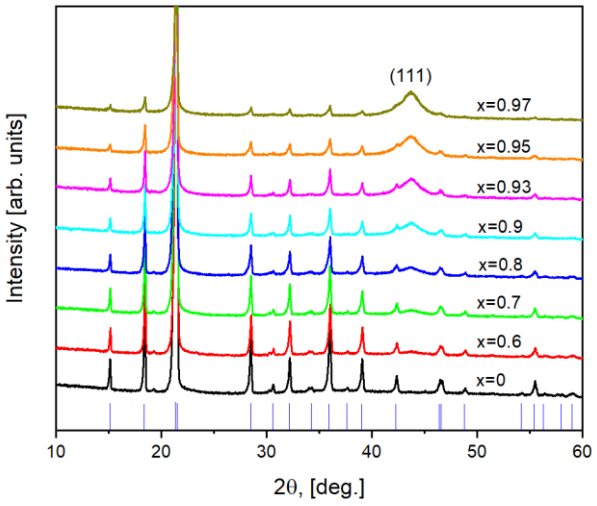

Figure 2 X-ray diffraction patterns of $(1–x)(CH_3)_4NBF_4 – xC_{ND}$ composites (blue dashes indicate the positions of the reflections according to PDF 482173).

In the random «salt-nanodiamond» mixture, the integral peak intensity (hkl) of the pure salt $I^0(hkl)$ should decrease in the composite as:

$$I(hkl) = I^0(hkl)(1-f). \quad (2)$$

The decrease in intensity of the experimentally obtained peaks with the volume fraction of nanodiamonds is sharper compared to a random mixture of components (Figure 3).

The intensity of the peaks may decrease due to the reduction of coherent scattering regions (*CSRs*). We used the Williamson-Hall method to determine the size of the *CSRs*, which takes into account the contribution of *CSRs* and microstresses to the peak broadening:

$$\beta\cos(\theta) = \frac{\lambda}{D} + 4\varepsilon\sin(\theta), \quad (3)$$

where β is the broadening (rad), λ = 0.15406 nm is the wavelength of Cu Kα radiation, D is the characteristic size of *CSRs* (nm), and ε is the magnitude of microstress (rad) [27]. The variation of the peak broadening with the angle 2θ is well described by the Williamson-Hall dependence for all samples (Figure 4). The *CSRs* of the samples depends only weakly on the composition (D = 70±10 nm), so the strong decrease in the intensity of the peaks is not related to the *CSRs*.

It can be assumed that $(CH_3)_4NBF_4$ transforms to the amorphous state on the surface of nanodiamonds, resulting in a decrease in the amount of crystalline phase contributing to diffraction. Previously, a similar effect was observed in other solid composite electrolytes "salt – insulator" [7, 21].

Figure 5 shows the morphology of the original salt (a), where individual particles smaller than 2 μm are visible; nanodiamonds (c), where the particle size is 3–15 μm; and typical morphology of the composites using the example of a tablet from the $0.2(CH_3)_4NBF_4–0.8C_{ND}$ composite.

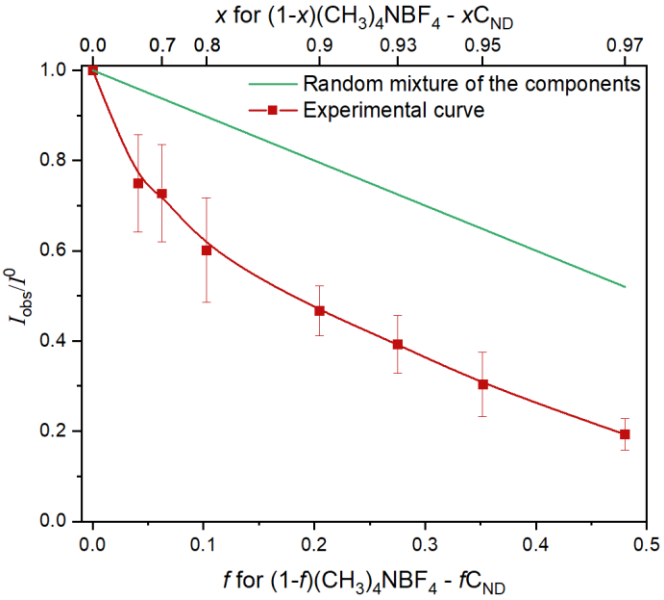

Figure 3 Variation of the relative intensity of the peaks with the volume fraction of nanodiamonds f: points on the experimental curve were determined by averaging the intensity of the peaks at 2θ = 15.2°, 18.5°, 21.4°, 28.5°.

 DOI: 10.15826/chimtech.2025.12.2.09

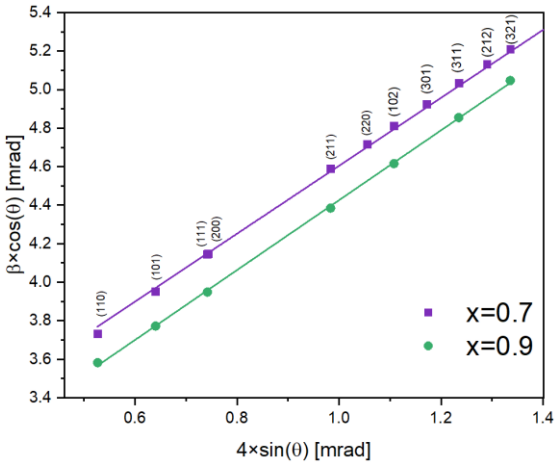

Figure 4 Williamson-Hall analysis for $(1–x)(CH_3)_4NBF_4$ – xC_{ND} (x = 0.7, 0.9): points are experimental data, lines are calculated.

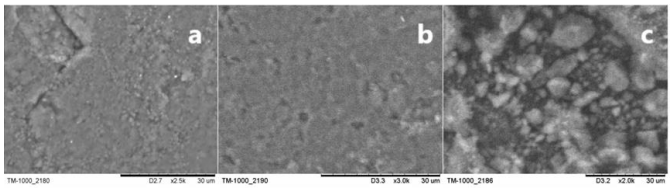

Figure 5 SEM images of $(CH_3)_4NBF_4$ (a), $0.2(CH_3)_4NBF_4$-$0.8C_{ND}$ composite (b), and nanodiamonds (c).

It can be seen that when the composites are pressed, dense tablets with a small number of pores are formed, which is consistent with the density data (the density of the tablets is ~90%); individual particles are poorly distinguishable.

3.3. Transport properties

Typical impedance hodographs are shown in Figure 6. The impedance hodographs were described by an equivalent circuit consisting of two impedances connected in series: the bulk impedance Z_{bulk}, which describes the resistance of the crystalline phase of the salt, and the electrode impedance Z_{el}, which describes the resistance at the electrolyte|electrode interface. The chosen equivalent circuit describes the observed impedance plots well (Figure 6).

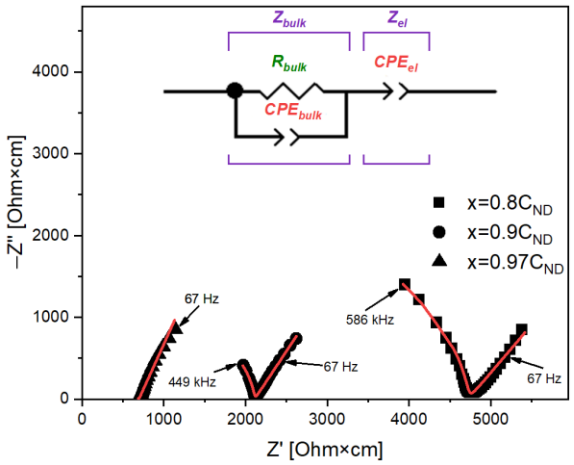

Figure 6 Typical impedance hodographs recorded for $(1–x)(CH_3)_4NBF_4$ – xC_{ND} (x = 0.8, 0.9, 0.97) at 250 °C. The approximate curves are shown in red. The equivalent circuit shown in the inset was used for modeling.

By analyzing the impedance hodographs, the temperature dependence of the conductivity was plotted (Figure 7). With increasing temperature, the conductivity of all composites increases, indicating the ionic nature of the conductivity. The dependences were well reproduced in heating-cooling cycles, thus the data obtained are at equilibrium.

For all compositions, the temperature dependence of the conductivity was well described by the Arrhenius equation:

$$\sigma T = Ae^{-\frac{E_a}{kT}}. \quad (4)$$

As the concentration of nanodiamonds in the composites increases, both the pre-exponential multiplier A and the activation energy E_a decrease (Table 1), indicating the appearance of new conduction channels with lower potential barriers to diffusion.

With increasing nanodiamond content, the conductivity of the composites increases monotonically by 3–5 orders of magnitude compared to the conductivity values obtained for the pure salt $(CH_3)_4NBF_4$ (Figure 8). The highest conductivity is characterized by the composite composition $0.03(CH_3)_4NBF_4$ – $0.97C_{ND}$ ($\sigma = 4.2 \cdot 10^{-3}$ S/cm at 300 °C).

The concentration dependence of «salt-inert additive» composites can be modeled using the previously proposed general mixing equation:

$$\sigma^{\alpha(f)} = \sigma_1^{\alpha(f)}(1 - f - f_s) + \sigma_s^{\alpha(f)} f_s + \sigma_{ND}^{\alpha(f)} f, \quad (5)$$

where σ_1, σ_s, σ_{ND} – conductivity of salt, amorphous salt layer and nanodiamonds, respectively; f_s and f – volume fraction of amorphous salt layer and nanodiamonds, respectively [7].

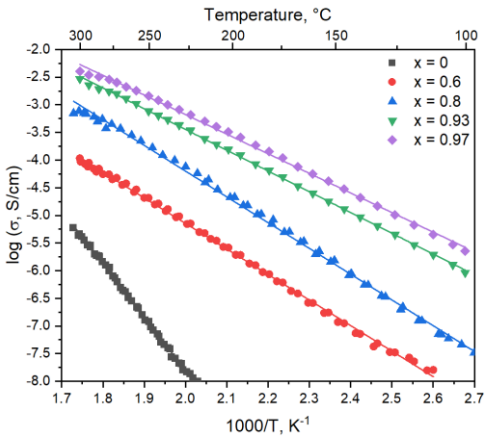

Figure 7 Temperature dependence of the specific conductivity σ of $(1–x)(CH_3)_4NBF_4$ – xC_{ND} in Arrhenius coordinates. The lines show approximate curves obtained from the Arrhenius equation.

Table 1 Conductivity parameters obtained by approximation with the Arrhenius equation.

xC_{ND}	fC_{ND}	E_a (eV)	log(A, S·K^{-1}·cm^{-1})
0	0	1.96±0.01	14.7±0.1
0.6	0.04	0.96±0.01	7.2±0.1
0.7	0.06	1.05±0.01	8.3±0.1
0.8	0.10	0.96±0.01	8.2±0.1
0.9	0.20	0.87±0.01	7.6±0.1
0.93	0.28	0.78±0.01	7.2±0.1
0.95	0.35	0.73±0.01	6.7±0.1
0.97	0.48	0.74±0.01	7.0±0.1

 DOI: 10.15826/chimtech.2025.12.2.09

The volume fraction of the amorphous salt layer stabilized by nanodiamonds was calculated according to Equation 6:

$$f_s = 6 \cdot \frac{\lambda}{L} \cdot f \cdot (1 - f) \qquad (f_s \le 1 - f), \qquad (6)$$

where L = 5.7 nm is the crystallite size of nanodiamonds estimated from the specific surface area of nanodiamonds, and λ is the thickness of the amorphous salt layer. The parameter $\alpha(f)$ depends on the composition, and a linear relationship was used for the calculations:

$$\alpha(f) = \alpha_1(1 - f) + \alpha_2 f, \qquad (7)$$

where 0 ≤ (α_1 and α_2) ≤ 1 are parameters that determine the morphology of the composite, which are independent of the composition.

The general mixing equation describes quite well the observed experimental values of conductivity at different temperatures (Figure 8). Table 2 summarizes the values of the calculated parameters, from which it can be seen that the conductivity of the amorphous layer is 4–5 orders of magnitude higher than that of the crystalline salt phase. Thus, the increase in conductivity is due to the formation of the amorphous salt phase.

For comparison, we took the published experimental data on the study of transport properties of composites with nanodiamonds and organic salts – tetrafluoroborates of substituted ammonium: $(C_4H_9)_4NBF_4$ ($T_{melting}$ = 162 °C) [22], $(C_4H_9)_3CH_3NBF_4$ ($T_{melting}$ = 158 °C) [28], $(C_2H_5)_3CH_3NBF_4$ ($T_{melting}$ = 320 °C) [29]. To date, the mechanism of ionic transport in such salts remains unknown. However, according to ^{19}F NMR data in $(C_4H_9)_4NBF_4$ the dominant charge carrier is BF_4^- anion, so we assume anionic character of conductivity in such salts [30].

Compared to other "organic salt – inert additive" systems, in the case of $(CH_3)_4NBF_4$, high conductivity values (more than 10^{-3} S/cm) are obtained at higher temperatures (>240 °C) (Figure 9). A trend is observed: in composites with fusible salts, high conductivity values are achieved at lower temperatures.

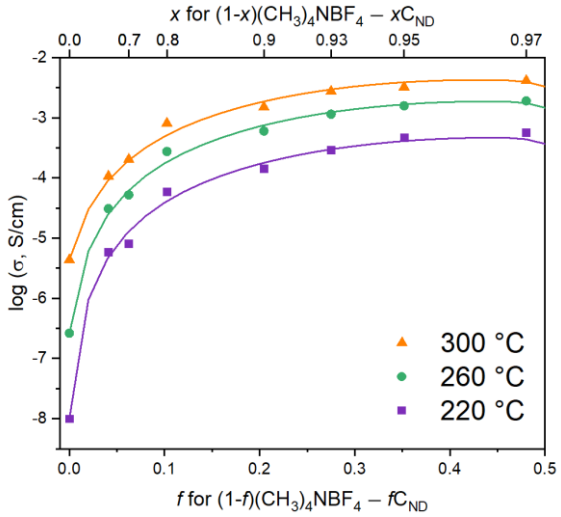

Figure 8 Dependence of the specific conductivity σ of $(1–x)(CH_3)_4NBF_4$ – xC_{ND} on the composition: points – experimental data, lines – approximation curves obtained from the mixing equation.

Table 2 Conductivity parameters of $(1–x)(CH_3)_4NBF_4$ – xC_{ND} composites obtained from the general mixing equation.

Parameter	220 °C	260 °C	300 °C
σ_1, S/cm	$1.0 \cdot 10^{-8}$	$2.6 \cdot 10^{-7}$	$4.4 \cdot 10^{-6}$
σ_s, S/cm	$5.0 \cdot 10^{-3}$	$2.0 \cdot 10^{-2}$	$4.0 \cdot 10^{-2}$
λ, nm		2.0	
α_1		0.35	
α_2		0.18	

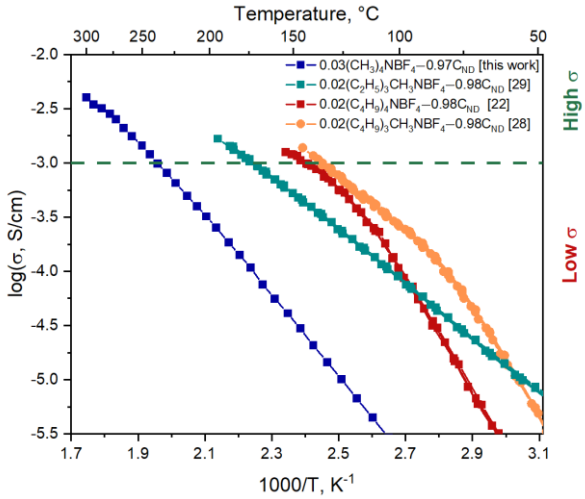

Figure 9 Comparison of transport properties of $0.03(CH_3)_4NBF_4$ – $0.97C_{ND}$ with other most conductive "organic salt-nanodiamond" composites according to [22, 28, 29].

4. Limitations

Solid composite electrolytes based on substituted ammonium salts with inert fillers are still poorly studied. The detailed mechanism of salt amorphization and the structure of the amorphous layer with atomic precision require further clarification, as well as the study of the detailed causes of the increased conductivity in composites.

5. Conclusions

The physicochemical properties of solid composite electrolytes $(1–x)(CH_3)_4NBF_4$ – xC_{ND} ($0 < x < 1$, x – molar fraction) have been studied for the first time. It was shown that the composites are thermally stable up to 300 °C. The decrease in the peak intensities in the XRD patterns of the composites is associated with their amorphization on the surface of nanodiamonds. It was shown that in composite electrolytes $(1–x)(CH_3)_4NBF_4$ – xC_{ND} with the increase in the proportion of nanodiamonds there is a monotonic increase in ionic conductivity up to x = 0.97 (f = 0.48, f – volume fraction), the maximum value is $\sigma = 4.2 \cdot 10^{-3}$ S/cm at 300 °C, which is 3–4 orders of magnitude greater than that of the original salt. The theoretical dependencies calculated using the mixing equation describe the experimental data well at temperatures 220, 260 and 300 °C. The conductivity of the amorphous layer $(CH_3)_4NBF_4$ in the phase contact region is 4–5 orders of magnitude higher than that of the original salt and makes the major contribution to the conductivity of the composites.

 DOI: 10.15826/chimtech.2025.12.2.09

Supplementary materials

No supplementary materials are available.

Data availability statement

All related data is incorporated in the manuscript. However, raw data which supports the finding of this study cannot be shared at this point in time, as the data forms part of ongoing study.

Acknowledgments

None.

Author contributions

Conceptualization: I.S., Y.M.
Data curation: I.S.
Formal Analysis: I.S.
Investigation: I.S.
Methodology: I.S., Y.M.
Project administration: N.U.
Resources: N.U.
Supervision: Y.M., N.U.
Validation: Y.M., N.U.
Visualization: I.S.
Writing – original draft: I.S.
Writing – review & editing: Y.M., N.U.

Conflict of interest

The authors declare no conflict of interest.

Additional information

Author IDs:
Ivan Stebnitskii, Scopus ID 58488613400;
Yulia Mateyshina, Scopus ID 6506782050;
Nikolai Uvarov, Scopus ID 7006949152.

Websites:
Institute of Solid State Chemistry and Mechanochemistry, http://www.solid.nsc.ru/en/institute/general/;
Novosibirsk State University, https://english.nsu.ru/.

References

1. Zhang Z, Wang X, Li X, Zhao J, Liu G, Yu W, Dong X, Wang J. Review on Composite Solid Electrolytes for Solid-State Lithium-Ion Batteries. Mater Today Sustain. 2023;21:100316. doi:10.1016/j.mtsust.2023.100316
2. Dirican M, Yan C, Zhu P, Zhang X. Composite Solid Electrolytes for All-Solid-State Lithium Batteries. Mater Sci Eng R Rep. 2019;136:27–46. doi:10.1016/j.mser.2018.10.004
3. Liu Q, Jiang L, Zheng P, Sun J, Liu C, Chai J, Li X, Zheng Y, Liu Z. Recent Advances in Stability Issues of Inorganic Solid Electrolytes and Composite Solid Electrolytes for All-Solid-State Batteries. Chem Rec. 2022;22(10):e202200116. doi:10.1002/tcr.202200116
4. Voropaeva DYu, Stenina IA, Yaroslavtsev AB. Solid-State Electrolytes: A Way to Increase the Power of Lithium-Ion Batteries. Russ Chem Rev. 2024;93(6):RCR5126. doi:10.59761/RCR5126
5. Xue S, Chen S, Fu Y, Zhu H, Ji Y, Song Y, Pan F, Yang L. Revealing the Role of Active Fillers in Li-ion Conduction of Composite Solid Electrolytes. Small. 2023;19(46):2305326.
6. Kumaravel V, Bartlett J, Pillai SC. Solid Electrolytes for High-Temperature Stable Batteries and Supercapacitors. Adv Energy Mater. 2021;11(3):2002869. doi:10.1002/aenm.202002869
7. Uvarov NF. Composite Solid Electrolytes: Recent Advances and Design Strategies. J Solid State Electrochem. 2011;15(2):367–389. doi:10.1007/s10008-008-0739-4
8. Liu S, Liu W, Ba D, Zhao Y, Ye Y, Li Y, Liu J. Filler-integrated Composite Polymer Electrolyte for Solid-state Lithium Batteries. Adv Mater. 2023;35(2):2110423.
9. Zheng F, Li C, Li Z, Cao X, Luo H, Liang J, Zhao X, Kong J. Advanced Composite Solid Electrolytes for Lithium Batteries: Filler Dimensional Design and Ion Path Optimization. Small. 2023;19(21):2206355. doi:10.1002/smll.202206355
10. Ponomareva VG, Bagryantseva IN, Shutova ES. Hybrid Systems Based on Nanodiamond and Cesium Dihydrogen Phosphate. Mater Today Proc. 2020;25:521–524. doi:10.1016/j.matpr.2020.01.304
11. Kubataev ZYu, Gafurov MM, Rabadanov KSh, Amirov AM, Akhmedov MA, Kakagasanov MG. The Effect of the Nanosized Oxide Filler on the Structure and Conductivity of Composite $(1 - x)(LiClO_4–NaClO_4)–xAl_2O_3$. Russ J Electrochem. 2023;59(8):598–603. doi:10.1134/S1023193523080050
12. Guseva AF, Pestereva NN, Kuznetsov DK, Boyarshinova AA, Gardt VA. Conductivity of Composites $MeWO_4–Al_2O_3$ (Me = Ca, Sr). Russ J Electrochem. 2023;59(4):284–290. doi:10.1134/S1023193523040079
13. Zhu H, MacFarlane DR, Pringle JM, Forsyth M. Organic Ionic Plastic Crystals as Solid-State Electrolytes. Trends Chem. 2019;1(1):126–140. doi:10.1016/j.trechm.2019.01.002
14. Pringle JM, Howlett PC, MacFarlane DR, Forsyth M. Organic Ionic Plastic Crystals: Recent Advances. J Mater Chem. 2010;20(11):2056. doi:10.1039/b920406g
15. Pringle JM. Recent Progress in the Development and Use of Organic Ionic Plastic Crystal Electrolytes. Phys Chem Chem Phys. 2013;15(5):1339–1351. doi:10.1039/C2CP43267F
16. MacFarlane DR, Forsyth M, Howlett PC, Kar M, Passerini S, Pringle JM, Ohno H, Watanabe M, Yan F, Zheng W, Zhang S, Zhang J. Ionic Liquids and Their Solid-State Analogues as Materials for Energy Generation and Storage. Nat Rev Mater. 2016;1(2):15005. doi:10.1038/natrevmats.2015.5
17. Thomas ML, Hatakeyama-Sato K, Nanbu S, Yoshizawa-Fujita M. Organic Ionic Plastic Crystals: Flexible Solid Electrolytes for Lithium Secondary Batteries. Energy Adv. 2023;2(6):748–764. doi:10.1039/D3YA00078H
18. Taniki R, Matsumoto K, Nohira T, Hagiwara R. All Solid-State Electrochemical Capacitors Using N,N-Dimethylpyrrolidinium Fluorohydrogenate as Ionic Plastic Crystal Electrolyte. J Power Sources. 2014;245:758–763. doi:10.1016/j.jpowsour.2013.07.020
19. Adebahr J, Ciccosillo N, Shekibi Y, Macfarlane D, Hill A, Forsyth M. The “Filler-Effect” in Organic Ionic Plastic Crystals: Enhanced Conductivity by the Addition of Nano-Sized TiO_2. Solid State Ionics. 2006;177(9–10):827–831. doi:10.1016/j.ssi.2006.02.022
20. Pringle JM, Shekibi Y, MacFarlane DR, Forsyth M. The Influence of Different Nanoparticles on a Range of Organic Ionic Plastic Crystals. Electrochim Acta. 2010;55(28):8847–8854. doi:10.1016/j.electacta.2010.08.027
21. Stebnitskii I, Mateyshina Y, Uvarov N. The Effect of Silicon Dioxide on the Structural, Thermal and Transport Properties of an Organic Ionic Plastic Crystal $(n\text{-}C_4H_9)_4NBF_4$. Chim Techno Acta. 2024;11(3):202411307.
22. Mateyshina Y, Stebnitskii I, Uvarov N. Composite Solid Electrolytes $(n\text{-}C_4H_9)_4NBF_4$–Nanodiamonds. Solid State Ionics. 2024;404:116419. doi:10.1016/j.ssi.2023.116419
23. Toby BH, Von Dreele RB. *GSAS-II* : The Genesis of a Modern Open-Source All Purpose Crystallography Software Package. J Appl Crystallogr. 2013;46(2):544–549. doi:10.1107/S0021889813003531
24. Zabinska G, Ferloni P, Sanesi M. On the Thermal Behaviour of Some Tetraalkylammonium Tetrafluoroborates. Thermochim Acta. 1987;122(1):87–94. doi:10.1016/0040-6031(87)80108-9
25. Matsumoto K, Harinaga U, Tanaka R, Koyama A, Hagiwara R, Tsunashima K. The Structural Classification of the Highly Disordered Crystal Phases of $[N_n][BF_4]$, $[N_n][PF_6]$, $[P_n][BF_4]$, and $[P_n][PF_6]$ Salts (N_n^+ = Tetraalkylammonium and P_n^+ = Tetraalkylphosphonium). Phys Chem Chem Phys. 2014;16(43):23616–23626. doi:10.1039/C4CP03391D

26. Giuseppetti G, Mazzi F, Tadini C, Ferloni P, Torre S. The Crystal Structure of Tetramethylammonìum Tetrafluoroborate,$(CH_3)_4NBF_4$, and the Disorder of the BF^-_4 Ion. Z fur Krist - Cryst Mater. 1992;202(1–4):81–88.
27. Himabindu B, Latha Devi NSMP, Rajini Kanth B. Microstructural Parameters from X-Ray Peak Profile Analysis by Williamson-Hall Models; A Review. Mater Today Proc. 2021;47:4891–4896. doi:10.1016/j.matpr.2021.06.256
28. Stebnitsky IA, Uvarov NF, Mateyshina YuG. Synthesis and Study of the Physicochemical Properties of Composite Solid Electrolytes $(C_4H_9)_3CH_3NBF_4$–$C_{nanodiamonds}$. Russ J Electrochem. 2024;60(1):18–24. doi:10.1134/S1023193524010105
29. Alekseev DV, Mateyshina YuG, Uvarov NF. Effect of Nanodiamond Additives on the Ionic Conductivity of the $(C_2H_5)_3CH_3NBF_4$ Organic Salt. Russ J Electrochem. 2022;58(7):594–599. doi:10.1134/S1023193522070035
30. Uvarov NF, Iskakova AA, Bulina NV, Gerasimov KB, Slobodyuk AB, Kavun VYa. Ion Conductivity of the Plastic Phase of the Organic Salt $[(C_4H_9)_4N]BF_4$. Russ J Electrochem. 2015;51(5):491–494. doi:10.1134/S102319351505016X

 DOI: 10.15826/chimtech.2025.12.2.09